Oligomeric States of the HIV-1 Integrase As Measured by Time-Resolved Fluorescence Anisotropy†

Eric Deprez,‡ Patrick Tauc,‡ Hervé Leh,§ Jean-François Mouscadet,§ Christian Auclair,‡,§ and Jean-Claude Brochon*,‡

Laboratoire de Biotechnologies et Pharmacologie Génétique Appliquée (UMR-CNRS 8532), Ecole Normale Supérieure (ENS) de Cachan, 61 avenue du Président Wilson, 94235 Cachan Cedex, France, and Laboratoire de Physicochimie et de Pharmacologie des Macromolécules Biologiques (UMR-CNRS 8532), Institut Gustave Roussy (IGR), 39 rue Camille Desmoulins, 94805 Villejuif Cedex, France

Received February 21, 2000; Revised Manuscript Received June 1, 2000

ABSTRACT: Self-assembly properties of HIV-1 integrase were investigated by time-resolved fluorescence anisotropy using tryptophanyl residues as a probe. From simulation analyses, we show that suitable photon counting leads to an accurate determination of long rotational correlation times in the range of 20−80 ns, permitting the distinction of the monomer, dimer, and tetramer from higher oligomeric forms of integrase. The accuracy of correlation times higher than 100 ns is too low to distinguish the octamer from other larger species. The oligomeric states of the widely used detergent-solubilized integrase were then studied in solution under varying parameters known to influence the activity. In the micromolar range, integrase exists as high-order multimers such as an octamer and/or aggregates and a well-defined tetramer, at 25 and 35 °C, respectively. However, integrase is monomeric at catalytically active concentrations (in the sub-micromolar range). Detergents (NP-40 and CHAPS) and divalent cation cofactors (Mg^{2+} and Mn^{2+}) have a clear dissociative effect on the high multimeric forms of integrase. In addition, we observed that Mg^{2+} and Mn^{2+} have different effects on both the oligomeric state and the conformation of the monomer. This could explain in part why these two metal cations are not equivalent in terms of catalytic activity in vitro. In contrast, addition of Zn^{2+} stimulates dimerization. Interestingly, this role of Zn^{2+} in the multimerization process was evident only in the presence of Mg^{2+} which by itself does not induce oligomerization. Finally, it is highly suggested that the presence of detergent during the purification procedure plays a negative role in the proper self-assembly of integrase. Accordingly, the accompanying paper [Leh, H., et al. (2000) *Biochemistry 39*, 9285−9294] shows that a detergent-free integrase preparation has self-assembly and catalytic properties different from those of the detergent-solubilized enzyme.

Human immunodeficiency virus type 1 (HIV-1)[1] integrase catalyzes both 3′-donor processing and strand transfer reactions, leading to the integration of the viral DNA into host chromosomal DNA. In vivo, these two reactions take place in two distinct compartments of the cell. The 3′-processing reaction occurs in the cytoplasm and consists of the specific cleavage of each 3′-LTR end dinucleotide of the viral DNA. The hydroxyl groups of recessed 3′-ends are then used in the nucleus in the strand transfer reaction transesterification to covalently join the viral and the target DNAs. In vitro, recombinant integrase is capable of separately catalyzing the 3′-processing and strand transfer reactions on short oligonucleotides that mimic the viral LTR termini (*1*).

HIV-1 integrase is a 32 kDa protein (288 amino acids) that includes three different functional domains, the N-terminus (residues 1−49), the central core (residues 50−212), and the C-terminus (residues 213−288). (i) The N-terminal domain contains a nonconventional HHCC zinc-finger motif. Numerous methods, including spectroscopy (*2*−*4*) and zinc blotting (*5*), have shown that this motif coordinates Zn^{2+} with a stoichiometry of one zinc per monomer. (ii) The central core domain, also called the catalytic core domain, contains the so-called D, D35, E motif (Asp 64, Asp 116, and Glu 152), conserved among retroviral integrases and transposases. This motif is essential for catalysis, and a single mutation of one of the three conserved acidic residues impairs the enzymatic activity (*6*−*9*). Furthermore, the central core domain is involved in binding of the viral DNA ends (*10*−*13*). (iii) The C-terminal domain contains the nonspecific DNA-binding activity of integrase and is involved in stabilizing the integrase−DNA complex

† This work was supported by grants from the SIDACTION, the Agence Nationale de Recherches sur le SIDA (ANRS), and the Centre National de la Recherche Scientifique (PCV program). E.D. is the recipient of a postdoctoral grant from the SIDACTION, and H.L. is the recipient of a postdoctoral grant from the ANRS.

* To whom correspondence should be addressed. Telephone: 33 1 47 40 27 17. Fax: 33 1 47 40 24 79. E-mail: brochon@lbpa.ens-cachan.fr.

‡ Ecole Normale Supérieure de Cachan.

§ Institut Gustave Roussy.

[1] Abbreviations: TFA, time-resolved fluorescence anisotropy; MEM, maximum entropy method; HIV, human immunodeficiency virus; LTR, long terminal repeat; CHAPS, 3-[(3-cholamidopropyl)dimethylammonio]-1-propanesulfonate (zwitterionic detergent); NP-40 or Nonidet P-40, ethylphenolpoly(ethylene glycoether)$_{11}$ (nonionic detergent); IN_{CHAPS}, integrase which is purified in the presence of the detergent CHAPS.

10.1021/bi000397j CCC: $19.00
Published on Web 07/14/2000

(*10*, *14*−*19*). Even though the structures of the three domains have been separately determined either by NMR or by X-ray crystallography (*20*−*26*), no structural data are available on the full-length integrase mainly due to its poor solubility. The three domains of integrase are strictly required for 3′-processing and strand transfer reactions (*6*). In vitro, a third reaction called disintegration can be observed. This reaction can be carried out by the central core alone (*5*, *27*). The different catalytic activities of integrase observed in vitro require a divalent metal cation as a cofactor which is coordinated by two residues of the catalytic triad (D64 and D116) (*23*, *26*). Although magnesium is considered to be the most relevant biological cofactor, manganese is preferred in in vitro activity assays.

Several studies suggest that the integrase functions as a multimer. One strong argument in favor of this hypothesis is that certain combinations of mutant integrase proteins, which are inactive individually, can restore the activity in vitro (*28*−*31*). The N-terminal domain bound to Zn^{2+} appears to play a key role in the multimerization process (*4*, *30*, *32*, *33*). This function of the N-terminal domain could explain why the presence of zinc in general enhances the catalytic activity (*4*, *32*). In the past, numerous techniques such as chemical cross-linking (*29*, *34*), size exclusion chromatography (*33*, *35*), and analytical ultracentrifugation (*4*, *33*, *35*) have been used to study the oligomerization properties of integrase in solution. Results were apparently contradictory depending on the protein concentration and the presence or absence of detergents and divalent cations (Mg^{2+}, Mn^{2+}, and Zn^{2+}). In particular, the protein concentrations required for these methods are relatively high compared to the catalytically active concentrations of integrase. Time-resolved fluorescence anisotropy (TFA) is a convenient tool, in particular for self-association studies of integrase, since its sensitivity allows detection of low protein concentrations in the range of those used in the enzymatic assays (submicromolar).

TFA is a powerful and useful method for investigating, via the determination of correlation times, molecular motions such as overall tumbling of a macromolecule as well as internal fluctuations (*36*, *37*). TFA has been extensively employed using tryptophanyl residues or an extrinsic fluorophore as the probe in many studies of proteins in solution, including folding reactions (*38*−*40*), the dynamics of domains (*41*−*44*), interactions with a ligand (*45*−*48*) or with nucleic acids (*49*−*53*), and self-assembly properties (*50*, *53*−*57*). Information about the oligomeric state of proteins can be obtained by determining the rotational correlation time which is related in a first approximation to the hydrated volume of the entire particle. An accurate determination of the rotational diffusion of the whole macromolecule using tryptophan fluorescence anisotropy decay is often a problem due to the rather short fluorescence lifetimes in comparison with the expected long correlation time of such a motion. On the other hand, the use of an extrinsic fluorophore could modify protein−protein interactions. In this paper, we will show that information about self-assembly of integrase can be obtained using time-resolved tryptophan fluorescence anisotropy with an appropriate photon counting statistics, and that we were able to discriminate between most of the different association states of integrase in solution.

Integrase purified in the presence of the detergent CHAPS for solubility reasons is widely used for in vitro studies. The CHAPS-solubilized integrase displays little or no Mg^{2+}-dependent activity at low protein concentrations, while it is highly active in the presence of Mn^{2+}, as shown in the accompanying paper (*73*). We were interested in determining both the oligomeric state of the CHAPS-solubilized integrase in the standard conditions used in enzymatic assays and the effects of divalent cations on the protein dynamics to gain a deeper insight into the relationship between the structural properties of integrase and the detection of the Mn^{2+}- or Mg^{2+}-dependent activity. In the simulation part, we performed analyses to predict a suitable and practicable photon counting level for accurate determination of long correlation times when using tryptophan fluorescence. In the experimental part, oligomeric states of the detergent-solubilized integrase are described under various conditions, e.g., protein and detergent concentrations, temperature, and the presence or absence of divalent cations. We found that monomer is the predominant form of integrase at a concentration of 0.2 μM in the presence of Mn^{2+}, under conditions where integrase is highly active. Zn^{2+} plays a role in the multimerization process, while Mn^{2+} and Mg^{2+} have a tendency to dissociate high-order multimeric forms. Furthermore, Mn^{2+} and Mg^{2+} display differential effects on the dissociation and also on the proper conformation of the monomer. On the other hand, detergents such as CHAPS or NP-40 were found here to perturb the quaternary structure of integrase. The accompanying paper (*73*) is devoted to the self-association and functional characterizations of a highly active integrase in the presence of Mg^{2+} when it is purified in the absence of any detergent.

MATERIALS AND METHODS

Protein Preparation. Integrase was a generous gift of Rhône Poulenc Rorer Co. (Vitry-sur-Seine, France). The protein was produced in *Escherichia coli* and purified in the presence of the detergent CHAPS (10 mM) as previously described (*58*, *59*). Dilution buffer for fluorescence measurements was 20 mM Tris-HCl (pH 7.2) and 1 mM DTT. The final CHAPS concentration was 1 mM. Nonionic Nonidet P-40 (NP-40) and zwitterionic CHAPS detergents were from Sigma.

Simulation of Time-Resolved Fluorescence Experiments. A computer program was developed to calculate the two polarized components of the protein fluorescence decay according to eqs 1 and 2:

$$I_{vv}(t) = \frac{1}{3}N E_\lambda(t) \otimes \left[\sum_{i=1}^{n} \alpha_i e^{-t/\tau_i}\left(1 + 2\sum_{j=1}^{m} \rho_j e^{-t/\theta_j}\right)\right] \quad (1)$$

$$I_{vh}(t) = \frac{1}{G}\left\{\frac{1}{3}N E_\lambda(t) \otimes \left[\sum_{i=1}^{n} \alpha_i e^{-t/\tau_i}\left(1 - \sum_{j=1}^{m} \rho_j e^{-t/\theta_j}\right)\right]\right\} \quad (2)$$

$$\text{with } \sum_{i=1}^{n} \alpha_i = 1$$

where $E_\lambda(t)$ is the time profile of the excitation pulse, α_i represents the proportion of fluorophores with the lifetime τ_i, and ρ_j represents the initial anisotropy of molecules with the rotational correlation time θ_j. The symbol $\otimes$ denotes a

convolution product. G is the correction factor for the difference in the monochromator transmission between parallel and perpendicular polarized components, and N is a scaling coefficient. The decay of the total fluorescence intensity is calculated from both polarized components by

$$T(t) = I_{vv}(t) + 2G \times I_{vh}(t) = NE_{\lambda}(t) \otimes (\sum_{i=1}^{n} \alpha_i e^{-t/\tau_i}) \quad (3)$$

We assume that each rotational correlation time is associated with all the fluorescence lifetimes. The anisotropy is then defined as

$$r(t) = \frac{I_{vv}(t) - G \times I_{vh}(t)}{I_{vv}(t) + 2G \times I_{vh}(t)} = \sum_{j=1}^{m} \rho_j e^{-t/\theta_j} \quad (4)$$

$$\text{with} \sum_{j=1}^{m} \rho_j = r_0$$

On the contrary, two-dimensional (τ_i and ρ_j) simulations should be performed (*54*, *60*). In this study, the tryptophanyl residues were excited at 296 nm where $r_0 = 0.25$.

For a spherical molecule, the rotational correlation time is related to its volume V by the relation

$$\theta = \frac{\eta V}{kT} \quad (5)$$

where η is the viscosity, T the absolute temperature, and k the Boltzman constant.

For a macromolecule having a fast internal flexibility, the anisotropy decay can be described by the following function:

$$r_j(t) = \rho_{f,j} e^{-t/\theta_{f,j}} + \rho_{s,j} e^{-t/\theta_{s,j}} \quad (6)$$

where θ_s and θ_f correspond to the overall motion (slow component) and to the local flexibility (fast component), respectively. On the basis of experimental results (see below), we assume that the internal flexibility is much faster than the tumbling ($\theta_f \ll \theta_s$). In addition, the local flexibility is not detected when the fitting time domain is started at $t \approx 4\theta_f$. In the case where local flexibilities are not taken into account, the apparent initial anisotropy for the overall motion is

$$r_0' = \sum_{j=1}^{m} \rho_{s,j} < r_0 \quad (7)$$

In this study, we used an r_0' of 0.15 on the basis of preliminary measurements.

Synthetic data were generated by a convolution product using a measured excitation time profile and the same conditions that were used for the experimental data collection (i.e., time scale, time resolution, and G-factor). A first set of simulated data was scaled to 1.2×10^6 and 1.6×10^6 counts for $I_{vv}(t)$ and $I_{vh}(t)$ decays, respectively. A second data set was scaled to 12×10^6 and 16×10^6 counts for $I_{vv}(t)$ and $I_{vh}(t)$ decays, respectively. For each calculated decay, two "mock" data were generated by adding either a Gaussian approximation of the Poisson noise or an experimental noise extracted from the analysis of two measured polarized decays [the corresponding residuals on $I_{vv}(t)$ and $I_{vh}(t)$ are shown in Figure 1]. That allows for the comparison of the influence of systematic errors on the results of the fitting procedure.

Time-Resolved Fluorescence Measurements. The time-resolved emission anisotropy was obtained by recording the two polarized emission decays $I_{vv}(t)$ and $I_{vh}(t)$, using the time-correlated single-photon counting technique. The excitation light pulse source was a Ti-sapphire sub-picosecond laser (Tsunami, Spectra Physics) associated with a third harmonic generator tuned at 296 nm. The repetition of the laser was set down to 4 MHz. The average output power of the laser at 296 nm was routinely 30 μW. If necessary, a neutral density filter was used to attenuate the excitation intensity. Fluorescence emission was detected through a monochromator (Jobin-Yvon model H10) set at 350 nm ($\Delta\lambda = 16$ nm) by a microchannel plate photomultiplier (Hamamatsu model R1564U-06) connected to a Phillips Scientific model 6954 amplifier (gain of 50). The excitation light pulse was triggered by a Hamamatsu photodiode (model S4753). The pulse signal was amplified, shaped, and connected to the stop input of the TAC (time amplitude converter, Ortec model 457) through a Tenelec model 453 discriminator. The function of the instrumental response of the laser pulse (100 ps) was recorded by detecting the light scattered by a water solution. The time scaling was 34.6 ps per channel, and 2048 channels were used. The two polarized components of the fluorescence decay and the instrumental response profile were alternatively collected during 90 and 30 s, respectively, over at least 20 periods until the total count of the I_{vv} component reached 12−16 million. To reduce the noise from the time−amplitude converter, the counting rate never exceeded 10 kHz. Correction for the monochromator transmission (G-factor $= I_{vv}/I_{vh}$) was determined from N-acetyl-tryptophanamide-polarized decays under the same conditions. The microcell (volume of 50 μL) was thermostated with a Haake type F3 circulating bath. The anisotropy decay parameters were extracted from both parallel $I_{vv}(t)$ and perpendicular $I_{vh}(t)$ polarized fluorescence decay components elicited by vertically polarized excitation. The corresponding analyses was performed by the quantified maximum entropy method (MEM) (*60*, *61*).

RESULTS

The aim of this study was to investigate the ability of tryptophan-polarized fluorescence to discriminate between the different self-association forms of HIV-1 integrase. Figure 1A shows one example of the typical fluorescence intensity decays of the two polarized components of integrase (1.8 μM, 25 °C), with the lifetime distribution (inset) as recovered by MEM analysis. The weighted residuals on $I_{vv}(t)$ and $I_{vh}(t)$ components and the corresponding autocorrelation curves are plotted in panels B−E of Figure 1.

Concentration-Dependent Distribution of Long Correlation Times of Integrase in Solution

To determine the oligomeric states of integrase in solution at the low concentrations used in enzymatic assays, we measured the correlation time distribution $\rho(\theta)$ at 25 °C in the protein concentration range of 1.8−0.045 μM (see Figure 2). The values obtained in the long correlation time domain (>10 ns) depend strongly on the protein concentration,

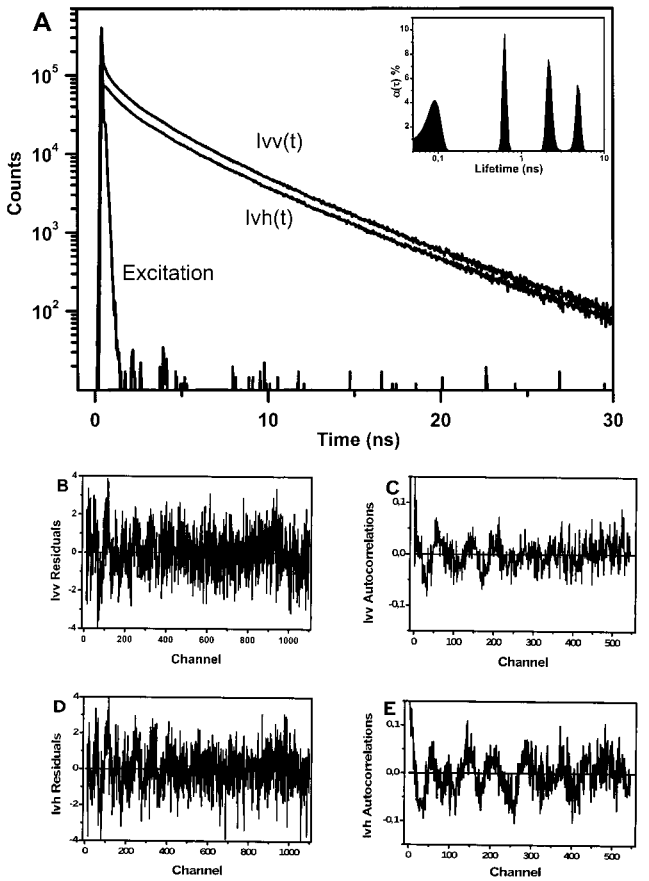

FIGURE 1: Measurements of the polarized emission decays, $I_{vv}(t)$ and $I_{vh}(t)$, of an integrase-containing sample. Experimental measurements were performed as described in Materials and Methods. The enzyme concentration was 1.8 μM, and the temperature was 25 °C. (A) The two experimental polarized fluorescence decays, $I_{vv}(t)$ and $I_{vh}(t)$, of the integrase. The excitation signal corresponds to the instrumental response of the laser pulse. (Inset) Lifetime distributions as recovered by the maximum entropy method (MEM). (B) Weighted residuals and (C) the corresponding autocorrelation curve of the $I_{vv}(t)$ decay; (D) weighted residuals and (E) the corresponding autocorrelation curve of the $I_{vh}(t)$ decay.

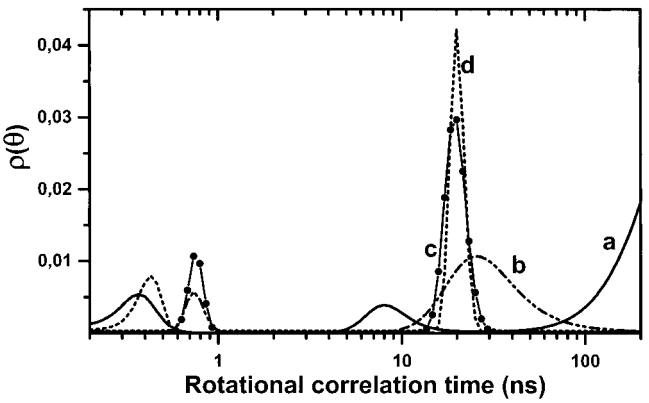

FIGURE 2: Concentration dependence of the rotational correlation time distributions of integrase at 25 °C: 1.8 (a), 0.36 (b), 0.18 (c), and 0.045 μM (d). Experimental measurements of rotational correlation times were performed as described in Materials and Methods.

whereas short correlation times, in the range of 400−800 ps, do not. Therefore, the internal flexibility of tryptophan residues is not directly related to the oligomeric state of the protein, and then, short correlation times are not very informative with respect to the quaternary structure of integrase. For the higher protein concentration (1.8 μM), an additional θ value of about 8 ns is necessary to obtain a satisfying data fit (see curve a in Figure 2). This additional correlation time seems to be related to the presence of aggregated forms in the sample (see below). We have no simple explanation for the finding of this rotational correlation time which was reproductible and thus seems to have a real physical meaning. Intermolecular tryptophan−tryptophan energy transfer cannot be ruled out and then could contribute to the depolarization process. We did not further explore this phenomenon.

Table 1: Excited-State Lifetimes of Integrase

[integrase] (μM)	τ_1 (ns)	τ_2 (ns)	τ_3 (ns)	τ_4 (ns)
1.8	0.08 (38%)	0.63 (21%)	2.18 (25%)	4.79 (16%)
0.36	0.09 (25%)	0.61 (25%)	2.03 (26%)	4.6 (23%)
0.18	0.11 (47%)	0.57 (24%)	1.95 (20%)	4.7 (10%)
0.045	0.15 (38%)	0.63 (26%)	1.80 (23%)	4.2 (13%)

In the time range of long rotational correlation times, a 1.8 μM concentrated IN_{CHAPS} solution exhibits a very broad pattern of $\rho(\theta)$ with values higher than 100 ns (see curve a in Figure 2). Taking the molecular mass of integrase (32 kDa) into account indicated that the solution contained high-order oligomeric forms of integrase. Decreasing the concentration to 0.36 μM induced a significant shift of $\rho(\theta)$ distribution to lower values with a maximum around 28 ns (see curve b of Figure 2), indicating a lower order of association states. In addition, the solution appeared to be heterogeneous in terms of molecular size as suggested by the broad shape of the distribution. In contrast, the sharp pattern of $\rho(\theta)$ at lower concentrations such as 0.18 and 0.045 μM suggested that these IN_{CHAPS} solutions are rather homogeneous (see curves c and d of Figure 2). Furthermore, the same oligomeric state was present in these two diluted solutions as suggested by the similar pattern of $\rho(\theta)$ leading to the identical θ value (19 ± 0.6 ns). This limit value could be reasonably attributed to the monomer (see the Discussion).

For HIV-1 integrase which contains seven tryptophans, four excited-state lifetime classes were found (see Table 1). These lifetime values were not significantly affected in a protein concentration range from 1.8 to 0.045 μM. Together with the determination of long rotational correlation times, this result means that the oligomeric state of the IN_{CHAPS} does not significantly influence the kinetics of emission of the tryptophans, suggesting that most of these residues are probably not directly involved in protein−protein interactions.

In time-resolved fluorescence studies, it is well-known that the accuracy of lifetime determinations is strongly dependent on the photon counting statistics (*60*, *62*). This point is also critical for the determination of rotational correlation times, especially in the case of mixtures of molecules having different sizes. Thus, we wondered whether time-resolved tryptophan fluorescence anisotropy and MEM analysis had the ability to recover and correctly resolve values of long correlation times, in the range of 20−200 ns as found experimentally. This question is fundamental for the interpretation of the TFA analyses in relation with the overall conformation of integrase and was approached using data simulations.

Analyses of Simulated Data

In this work, two classes of $\rho(\theta)$ distributions have been observed depending on the experimental conditions. The first one corresponds to sharp peaks centered at about 20, 40, or 80 ns. The second one corresponds to the not well-defined broad and flat peaks, characterized by a centroid position at 28, 60, or >100 ns. Therefore, simulations were performed to determine, first, the accuracy of the correlation time measurements for a given condition of photon counting and, second, the ability of TFA coupled to MEM analysis to separate two peaks from the $\rho(\theta)$ distribution in the case of a mixture of oligomers. Since the fluorescence decay of the tryptophan residues is not significantly affected by the state of association of the protein, we used an average of lifetime compositions to generate the "mock" data. The very short lifetime of about 80 ps vanishes 400 ps after excitation and then cannot report for the overall motion of the protein. Thus, we used only three fluorescence lifetimes in our simulations: 0.6, 2.1, and 4.7 ns with relative contributions of 35, 40, and 25%, respectively. The corresponding average lifetime was 2.3 ns. We have constructed couples of polarized fluorescence decays for molecular species having single correlation times of 20, 40, and 80 ns, respectively. These values were found experimentally as mentioned above, and the rotational correlation time of 20 ns can be reasonably attributed to the integrase monomer (see the Discussion). Correlation times of 120 or 160 ns were used to simulate high-order oligomeric forms. The predicted value of the initial anisotropy (r_0) which is related to the overall rotation should be 0.25 for an excitation at 296 nm (*63*). In our case, experimental data analysis showed the presence of initial fast depolarization due to the local flexibility of tryptophans. The initial anisotropy used in the simulation when taking into account only the slow rotational motion was 0.15 (r_0' as defined by eq 7). The influence of counting statistics [1.2×10^6 and 1.6×10^6 counts or 12×10^6 and 16×10^6 counts for $I_{vv}(t)$ and $I_{vh}(t)$ decays, respectively] as well as the nature of the noise (experimental or random) on the determination of the rotational correlation time have been tested.

The results of MEM analyses of simulated data are shown in Figure 3. The correponding values of the peak centroid and accuracies are given in Table 2. In the case of simulation of a single component (see panels A−D of Figure 3), the MEM analysis can recover a correct value of the expected rotational correlation time of the monomer ($\theta = 20$ ns) (curve a), regardless of the counting statistics or the noise. The accuracy on $\theta = 40$ ns (curve b) determination is not very satisfying at low counts but is strongly improved by increasing the counts by a factor of 10, with experimental or random noise (compare panels A and B of Figure 3, and panels C and D of Figure 3). When the input correlation time is 80 ns (curve c), a low counting statistics in all noise conditions led to a very poor determination of the peak centroid (see panels A and C of Figure 3). In contrast, a high counting (see panels B and D of Figure 3) may allow for the identification of the 80 ns correlation time with a reasonable accuracy. For correlation times of >100 ns (curves d and e), even countings of 12×10^6 and 16×10^6 of photons on the vertical and horizontal components, respectively, do not allow for the recovery of correct values. In other words, oligomeric forms of integrase higher than tetramer cannot be distinguished from each other. In mixtures with equal concentrations of two molecular species, characterized for instance by rotational correlation times of 20 and 40 ns, respectively (Figure 3E), or 40 and 80 ns, respectively (data not shown), simulation analysis led to a single broad peak instead of two sharp separated peaks. The values of centroids were intermediary (about 30 and 60 ns, respectively) and correspond to average values of the two long correlation times that characterized the individual molecules. On the basis of simulation results, the experimental measurements of correlation times shown in this work were taken with high photon counting conditions, around 12×10^6 and 16×10^6 counts on the vertical and horizontal components, respectively.

Modulation of Integrase Self-Assembly

Temperature Effect. Increasing the temperature from 10 to 35 °C dissociated the aggregated form of IN_{CHAPS} observed at 1.8 μM, to a homogeneous form characterized by a correlation time of 70 ns (see Figure 4). The slight difference between $\rho(\theta)$ measured at 30 and 35 °C (compare curves c and d) is explained by temperature and viscosity effects on the tumbling of a macromolecule in solution (see eq 5). To compare the θ values obtained at different temperatures, a correction taking into account the temperature and the viscosity changes was required according to the Stokes−Einstein equation. When applied to θ at 30 and 35 °C, the correction led to similar θ values (80 ns) calculated for a temperature of 25 °C. As already observed in Figure 2 (curve a), the θ value found at about 10 ns was related to the presence of aggregated forms of integrase in solution (see curves a and b of Figure 4).

Detergent Effect. To measure the effect of detergent concentration on the aggregated form of integrase, we selected conditions which were optimal for the generation of aggregates: high concentration of integrase (1.8 μM) and low temperature (10 °C). From 0.01 to 0.09% (v/v) nonionic detergent NP-40, aggregates (θ > 300 ns) were efficiently dissociated in achieving an oligomeric form characterized by a rather symmetric and sharp pattern of $\rho(\theta)$ and a temperature-corrected θ value of 40 ns (see Figure 5). A similar result was found using the detergent CHAPS from 1 to 11.7 mM (data not shown). At 25 °C, a NP-40 concentration of 0.05% (v/v) yielded the monomeric form ($\theta = 20$ ns) (data not shown), indicating synergistic effects of temperature and detergent on the complete dissociation of integrase.

Effects of Divalent Cations. Effects of activity cofactor Mn^{2+} and Mg^{2+} on the self-assembly and conformation state of IN_{CHAPS} were tested on both the aggregated (Figure 6A) and monomeric (Figure 6B) forms. As mentioned above, the integrase at 1.8 μM is characterized by high-order multimeric states (θ > 100 ns) (Figure 6A, curve a). Addition of 10 mM Mn^{2+} induced the dissociation of large molecular assembly species to another multimeric form characterized by a well-defined $\rho(\theta)$ centered at 80 ns (Figure 6A, curve b). The same concentration of Mg^{2+} yielded a stronger effect on the oligomer dissociation of the IN_{CHAPS} than Mn^{2+} (Figure 6A, curve c). In fact, in the presence of 10 mM Mg^{2+}, the position of the centroid was shifted to lower values (about 60 ns). On the other hand, the solution displayed a broad

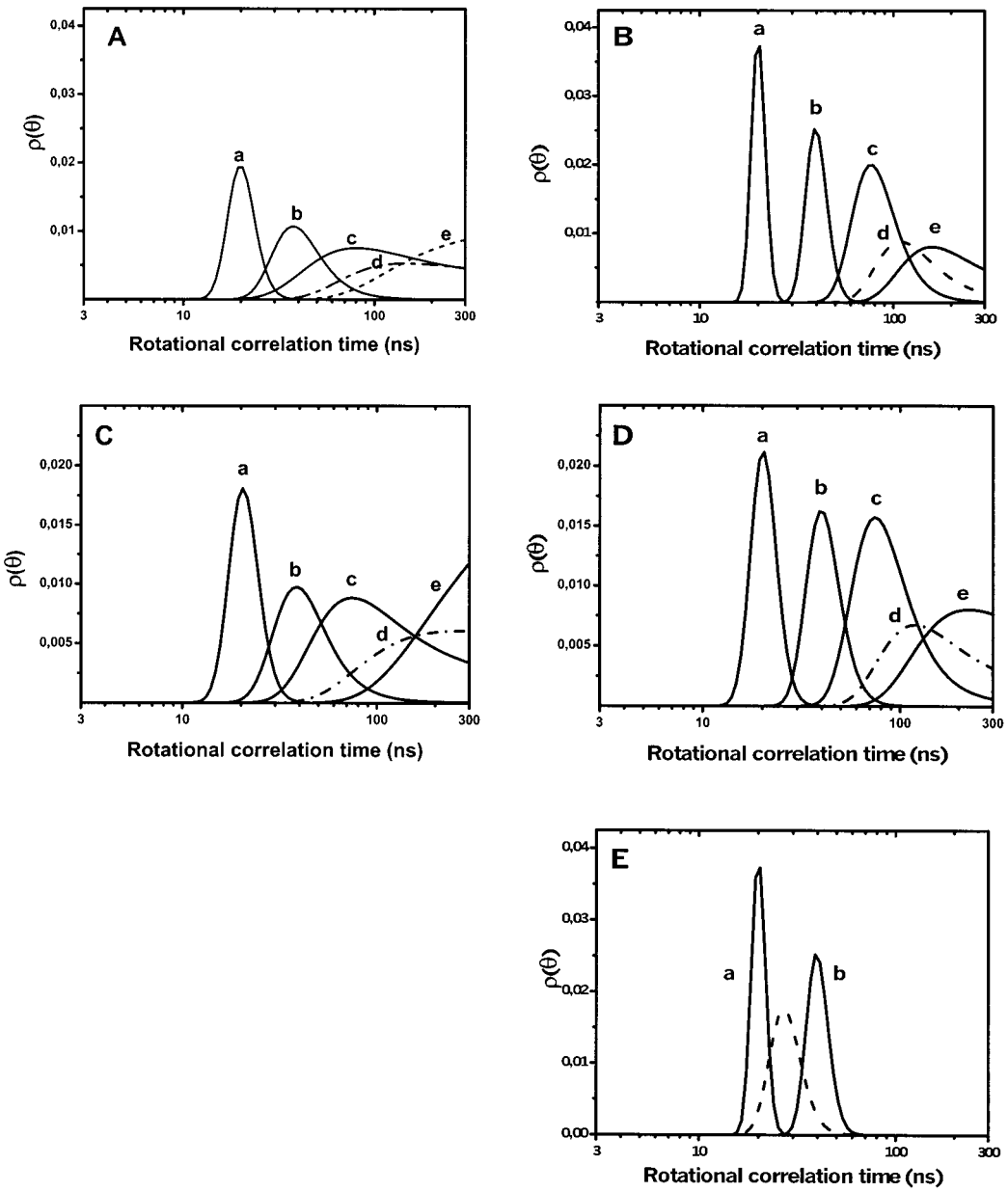

FIGURE 3: Influence of the counting statistics and the type of noise on the recovery of rotational correlation times from simulated polarized decays. (A−D) Single input values of 20 (a), 40 (b), 80 (c), 120 (d), and 160 ns (e). (A and C) Low counting statistics (1.2×10^6 and 1.6×10^6 counts on the vertical and horizontal components, respectively). (B and D) High counting statistics (12×10^6 and 16×10^6 counts on the vertical and horizontal components, respectively). (A and B) Experimental noise (extracted from the residuals shown on Figure 1). (C and D) Gaussian noise. (E) Simulation data analysis of a mixture (50%/50%) of two input correlation times (20 and 40 ns) under conditions of high counting statistics and experimental noise (- - -). Single input values of 20 (a) and 40 ns (b) (—).

Table 2: Simulation Data Analyses

	output value of θ (ns) [width (ns)]			
	random noise[a]		experimental noise[b]	
input value of θ (ns)	low counting[c]	high counting[d]	low counting[c]	high counting[d]
20	20.6 ± 1.4 (3.5)	20.2 ± 0.4 (1.7)	21.2 ± 1.7 (3.9)	20.7 ± 0.9 (3.2)
40	45 ± 19 (20)	40.6 ± 2.2 (5.4)	48 ± 24 (24)	42 ± 5 (9.3)
80	118 ± 48 (71)	88 ± 21 (30)	113 ± 48 (65)	94 ± 29 (41)
120	151 ± 59 (70)	134 ± 41 (52)	165 ± 60 (70)	148 ± 46 (62)
160	188 ± 58 (66)	175 ± 43 (58)	205 ± 58 (62)	190 ± 44 (61)
20/40 (50%/50%)	29 ± 5 (8)	28.8 ± 3.2 (7.5)	31 ± 8.5 (11)	31 ± 8.6 (13)

[a] Gaussian approximation of a Poisson noise. [b] From the experimental residuals shown in Figure 1. [c] A total of 1.2×10^6 and 1.6×10^6 counts for $I_{vv}(t)$ and $I_{vh}(t)$ decays, respectively. [d] A total of 12×10^6 and 16×10^6 counts for $I_{vv}(t)$ and $I_{vh}(t)$ decays, respectively.

$\rho(\theta)$ distribution characteristic of a mixture of different multimeric forms (probably a mixture of two major components, $\theta = 40$ and 80 ns, as suggested by simulations). The effects of these divalent cations on a monomeric protein

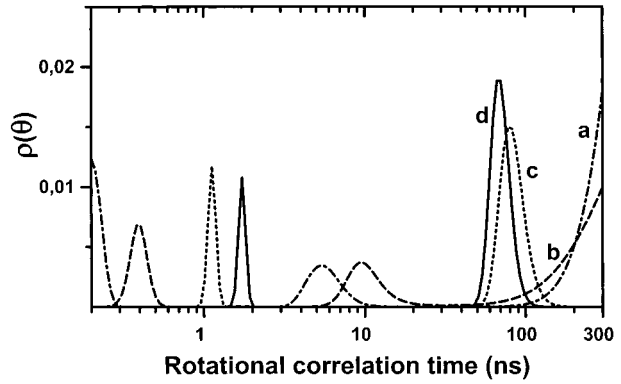

FIGURE 4: Temperature dependence of the rotational correlation time distributions of integrase at 10 (a), 25 (b), 30 (c), and 35 °C (d). The enzyme concentration was 1.8 μM. Experimental measurements of rotational correlation times were performed as described in Materials and Methods.

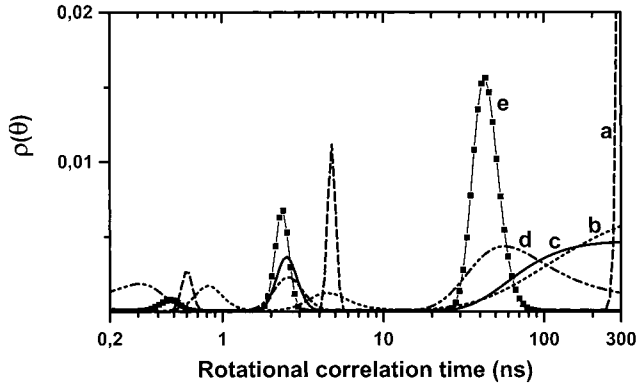

FIGURE 5: Effect of the detergent NP-40 on the self-assembly of integrase at 10 °C. No detergent (a), 0.01% (v/v) NP-40 (b), 0.024% (v/v) NP-40 (c), 0.05% (v/v) NP-40 (d), and 0.09% (v/v) NP-40 (e). The protein concentration was 1.8 μM. Experimental measurements of rotational correlation times were performed as described in Materials and Methods.

at 25 °C are shown in Figure 6B. Increasing or decreasing the temperature had no effect on the monomeric form (data not shown). Mg^{2+} (curve c) but not Mn^{2+} (curve b) led to a significant and reproductible decrease in the overall protein volume ($\theta = 16 \pm 0.4$ ns instead of 19 ± 0.6 ns) which could be interpreted as a contraction of the monomer. A similar effect of Mg^{2+} was also observed on the catalytic core of HIV-1 integrase (unpublished results).

In the presence of zinc, the rotational dynamics of the monomeric structure was not significantly modified with respect to the usual θ value of 19 ns (Figure 7, compare curves a and c). In contrast, in the presence of Mg^{2+} which is not capable by itself of inducing oligomerization of the integrase (curve b), Zn^{2+} stimulated self-association of the protein (curve d). This result was not obtained using Mn^{2+} (data not shown).

DISCUSSION

The time-resolved tryptophan fluorescence anisotropy technique has several advantages for studying the self-assembly properties of integrase. Its detection sensitivity allows for the performance of measurements using protein concentrations in the $10^{-8}-10^{-7}$ M range. This is much lower than the concentrations used for protein−protein cross-linking, size exclusion chromatography, or analytical ultra-

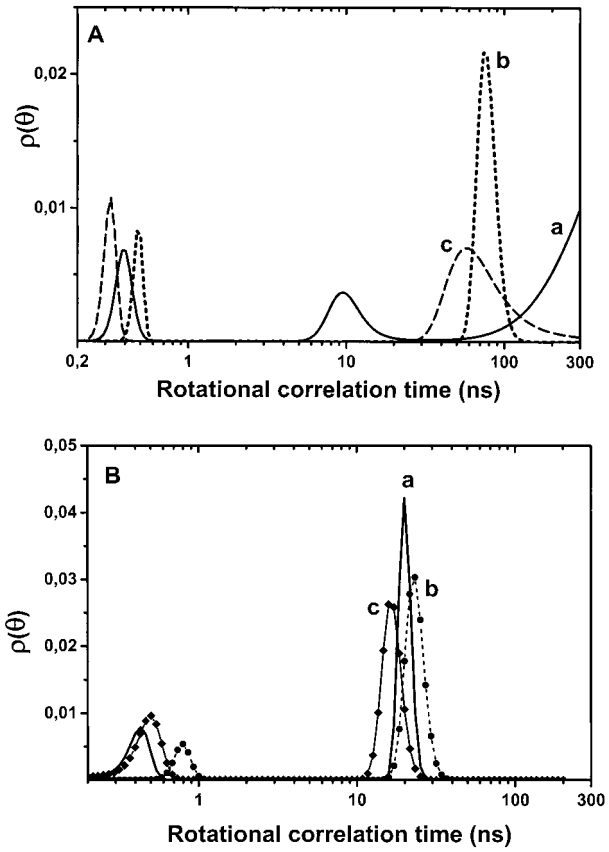

FIGURE 6: Effects of Mn^{2+} or Mg^{2+} on the oligomerization and the hydrated volume of integrase at 25 °C: enzyme alone (a) and with 10 mM Mn^{2+} (b) and 10 mM Mg^{2+} (c). The protein concentration was 1.8 (A) or 0.18 μM (B). Experimental measurements of rotational correlation times were performed as described in Materials and Methods.

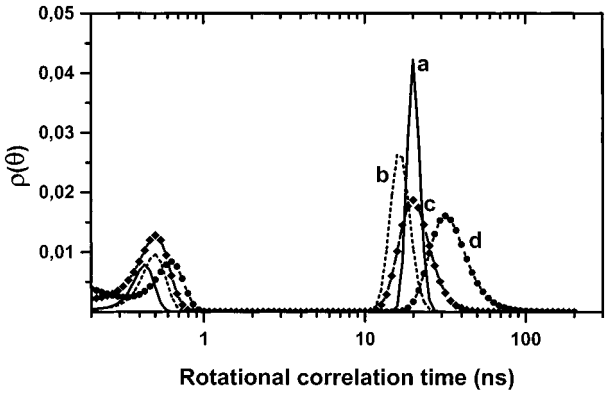

FIGURE 7: Effect of Zn^{2+} on the oligomerization of integrase at 25 °C: enzyme alone (a) and with 10 mM Mg^{2+} (b), 10 μM Zn^{2+} (c), and 10 mM Mg^{2+} and 10 μM Zn^{2+} (d). The protein concentration was 0.18 μM. Experimental measurements of rotational correlation times were performed as described in Materials and Methods.

centrifugation (usually in the micromolar range). Therefore, for the first time, information about the oligomeric states of integrase in solution can be obtained under conditions of protein concentrations which are routinely used in enzymatic assays, i.e., 40−200 nM. Experimentally, the photon counting required for accurate determination of long correlation times (in this study, 12×10^6 and 16×10^6 counts on the vertical and horizontal components, respectively) was typically performed for 1−1.5 h, which is similar to the incubation time used in the enzymatic assays (typically 1 h). The

acquisition time is thus reasonable, and neither an oligomerization drift nor a photobleaching phenomenon was observed. On the other hand, using intrinsic tryptophan fluorescence is of great interest since it does not result in pertubation to the oligomerization state that may be caused by attachment of extrinsic fluorophore to the protein.

In this study, we clearly determined three rotational correlation times for integrase that depended on the experimental conditions: 20, 40, and 80 ns. First, it is highly probable that the correlation time found at 20 ns corresponds to the overall tumbling of the monomer since no dilution effect was observed on this value from 200 to 45 nM integrase. This is consistent with the apparent K_d value ($1.85-2.5 \times 10^{-5}$ M) for the dimer dissociation found by others (*33*, *64*). The value of the rotational correlation time expected for a globular 32 kDa protein is approximatively 13.5 ns at 25 °C, assuming a partial specific volume of 0.73 mL/g and a typical hydration level of 50%. The discrepancy between the calculated and the observed values can be attributed to a nonspherical geometry of the monomer leading to an axis ratio of 2.5 (for randomly orientated chromophores). Second, it is reasonable to assume that the correlation time found at 40 ns corresponds to the dimer of integrase (MW of 64 kDa). This is substantiated by the absence in this study of any well-defined peak between 20 and 40 ns. Moreover, serum albumin (MW of 66 kDa) displays a similar rotational correlation time of 41.7 ns (*65*). Finally, the rotational correlation time found around 80 ns cannot be clearly attributed to the tetramer on the basis of predictive calculations. In fact, as the degree of oligomerization of integrase increases, significant changes in both the overall hydration and the geometry of the protein assembly are to be expected. Therefore, the value of 80 ns could also be attributed to a trimeric form. Nevertheless, to our knowledge, the trimeric form of the integrase has been detected together with the tetramer in only one study (*34*), whereas in many other studies, monomer, dimer, and tetramer, but not trimer, have been observed (*4*, *29*, *33*, *35*). Thus, we hypothesise here that the one well-defined rotational correlation time found in the 60−100 ns range more likely corresponds to the tetrameric form, which has been systematically detected by other techniques.

Accurate determination of long correlation times, as expected for the high-order oligomeric forms of integrase, is obviously limited and may be subject to controversy mainly due to the relatively short lifetimes of tryptophan residues, as observed for integrase (Table 1). What is the limit of this appoach in our study? Simulation analysis demonstrates that pure monomeric species can be clearly defined even with lower photon counting (1.2×10^6 and 1.6×10^6 counts for I_{vv} and I_{vh} decays, respectively). Under these conditions, the recovery of the dimer is not very satisfying and the tetramer is absolutely not well-defined. In contrast, a 10-fold higher level of photon counting on each component allows for a better determination of the correlation times of both dimer and tetramer. These high-counting experiments are now currently available due to the high excitation intensity generated by solid-state lasers. In the case of high photon counting, it is also possible to distinguish tetramer ($\theta = 80$ ns) from higher oligomeric states ($\theta >$ 100 ns) but it is difficult to precisely describe the exact nature of these large multimers (hexamers, octamers, ..., aggregates). In other words, we cannot tell from our study if an octameric form really exists in solution as has been previously suggested (*33*). We have also looked at mixtures of oligomeric states in the same sample. Analyses of simulated data of mixtures of either monomer and dimer (50%/50%) or dimer and tetramer (50%/50%) under conditions of high photon counting do not permit separation of the two corresponding correlation times in the $\rho(\theta)$ distribution. Instead, intermediary peaks were observed: 30 and 60 ns for the monomer/dimer and dimer/tetramer mixtures, respectively. In both cases, a much higher photon counting would be required to separate the two molecular species which would lead to unreasonable acquisition times. The θ values of 30 and 60 ns, as recovered experimentally from broad peaks, very likely correspond to such mixtures.

Studies on different types of integrases strongly support the role of the multimerization process in its catalytic activity. In this paper, we found that integrase purified in the presence of detergent is homogeneous and monomeric at catalytically active concentrations, between 40 and 200 nM. Moreover, the Mn^{2+}-bound monomer of IN_{CHAPS} is highly active, whereas the Mg^{2+}-bound monomer is not (*73*). One hypothesis is that Mn^{2+}-dependent activity can occur when the protein is in a monomeric state, whereas the more physiological Mg^{2+}-dependent activity absolutely requires a higher-order oligomeric form. However, it is difficult to reconcile this hypothesis with activity complementation studies in the presence of Mn^{2+} performed with CHAPS-containing samples of sub-micromolar pairs of integrase mutant proteins, which are by themselves inactive (*29*). A second hypothesis is that both Mn^{2+}- and Mg^{2+}-dependent activities require integrase as a multimer; in this hypothesis, substrate DNA could organize Mn^{2+}-bound monomers into a multimeric active form, according to Heuer and Brown (*66*) and Pemberton et al. (*67*). This organization could not occur at sub-micromolar concentrations in the case of the Mg^{2+}-bound monomer. Since we have unambiguously shown that IN_{CHAPS} is monomeric in solution, these different studies taken together strongly suggest that the Mn^{2+}-bound monomeric protein is capable of recognizing the DNA substrate and then forming a functional multimer in a DNA-dependent manner. TFA studies of the self-association of integrase bound to viral DNA are in progress to directly test this model. Why is a monomeric form in the presence of Mg^{2+} unable to multimerize in the same manner? Magnesium is considered the relevant biological cofactor, and numerous studies show that both metal divalent cations Mg^{2+} and Mn^{2+} are not equivalent in terms of activity (*10*, *68*, *69*, *73*). Our study provides evidence that they also have clearly different effects on the integrase structure. First, Mn^{2+} is less able to promote the dissociation of high multimeric states than Mg^{2+}. It appears that addition of Mn^{2+} leads to a well-defined tetramer, whereas protein in the presence of Mg^{2+} is characterized by several suboligomers such as dimers and tetramers. This dissociation effect does not appear to be related to ionic strength since aggregates are resistant to NaCl concentrations up to 1 M (data not shown). It is therefore likely that the dissociation effect of these divalent cations we have observed is specific and is due to a conformational change of the protein. In this paper, we showed a differential effect of both cations on the tertiary structure of integrase. The monomer in the presence of Mg^{2+} systematically has a

rotational correlation time around 16 ns instead of 19 ns. This indicates a rigidification effect of Mg^{2+} on the dynamics of the protein. This effect is not observed with Mn^{2+}. It has been previously shown that binding of the divalent cation Mn^{2+} or Mg^{2+} induces a conformational change in the integrase structure as probed by monoclonal antibodies or proteolytic enzymes (*70*, *71*). It seems from our results that the hydrated volume and then the overall geometry of the monomeric integrase are not sensitive to such a conformational change in the presence of Mn^{2+}. In contrast, the conformational change which occurs with Mg^{2+} could have a direct consequence on the hydrodynamic property of integrase. Thus, a differential conformational change on each subunit of the multimer could be responsible for the differential effect of both divalent cations on the quaternary structure of integrase. This could explain the different abilities of Mg^{2+} and Mn^{2+} to favor multimeric states of IN_{CHAPS} on DNA. Mn^{2+}, which promotes less dissociation, yields the more efficient complex for the catalysis. Note that the differential effects of Mg^{2+} and Mn^{2+} on the integrase conformation could also lead to a less stable integrase−DNA complex in the presence of Mg^{2+}, according to Pemberton et al. (*67*). Thus, we cannot neglect the fact that the integrase multimerization on the viral DNA nucleation site is more likely to occur under favorable conditions of free energy binding (in the presence of Mn^{2+}), independent of our observation that the two divalent cations have diffential effects on the protein self-assembly in the absence of DNA. This point has been explored in the accompanying paper (*73*) where it is shown that IN_{CHAPS} displays different DNA binding properties depending on the nature of the divalent cation.

Zinc is not considered to be a cofactor, but on the basis of static fluorescence anisotropy (*33*) and size exclusion chromatography experiments (*4*), it has been suggested that zinc enhances the catalytic activity of integrase by stimulation of self-association. In our study, we directly observed stimulation of dimerization after the addition of Zn^{2+}. This effect was Mg^{2+}-dependent and did not occur in the presence of Mn^{2+}. Therefore, the presence of zinc could counteract the stronger effect of Mg^{2+} on the multimer dissociation. Our results are consistent with those of Lee and Han (*32*), who have shown that Mg^{2+}-dependent activity is stimulated by Zn^{2+} whereas Mn^{2+}-dependent activity is not altered in the presence of Zn^{2+}.

Detergent is often present during protein purification to aid in the solubilization of integrase. However, the detergent may also perturb the multimeric state of the protein, inducing dissociation of protein−protein interactions. Effectively, we found that multimeric states of integrase are strongly modified by varying the detergent concentration. NP-40 or CHAPS results in similar degrees of dissociation of high-order oligomerics of integrase and in addition seems to change the nature of protein−protein interactions. In fact, with the initial concentration of the detergent CHAPS (1 mM), the increase in temperature from 10 to 30 °C dissociates the high-order multimeric states, resulting in a well-defined tetramer. This tetramer is rather stable versus temperature since no variation in the self-assembly was observed between 30 and 35 °C. On the other hand, no temperature effect was observed on the monomer between 10 and 35 °C. Taken together, these results indicate a minor contribution of the enthalpy in the monomer−dimer−tetramer transition. A similar result was recently obtained with the ASV integrase (*72*). In contrast, after the addition of 0.05% (v/v) NP-40, we observed that the integrase sample is characterized by a dimer−tetramer equilibrium at 10 °C whereas it displays a homogeneous monomeric form at 25 °C. Thus, it seems that the presence of detergent favors an enthalpic contribution that does not really exist in pure aqueous solvent and could disturb both self-assembly organization of integrase and Mg^{2+}-dependent activity. This point is further discussed in the accompanying paper in which integrase purified in the total absence of detergent is (i) characterized by different multimeric states compared to the detergent-solubilized enzyme and (ii) highly active in the presence of Mg^{2+} even at sub-micromolar protein concentrations.

REFERENCES

1. Brown, P. O. (1997) in *Retrovirus* (Coffin, J. M., Hughes, S. H., and Varmus, H. E., Eds.) pp 161−203, Cold Spring Harbor Laboratory Press, Plainview, NY.
2. Burke, C. J., Sanyal, G., Bruner, M. W., Ryan, J. A., LaFemina, R. L., Robbins, H. L., Zeft, A. S., Middaugh, C. R., and Cordingley, M. G. (1992) *J. Biol. Chem. 267*, 9639−9644.
3. Haugan, I. R., Nilsen, B. M., Worland, S., Olsen, L., and Helland, D. E. (1995) *Biochem. Biophys. Res. Commun. 217*, 802−810.
4. Zheng, R., Jenkins, T. M., and Craigie, R. (1996) *Proc. Natl. Acad. Sci. U.S.A. 93*, 13659−13664.
5. Bushman, F. D., Engelman, A., Palmer, I., Wingfield, P., and Craigie, R. (1993) *Proc. Natl. Acad. Sci. U.S.A. 90*, 3428−3432.
6. Drelich, M., Wilhelm, R., and Mous, J. (1992) *Virology 188*, 459−468.
7. Engelman, A., and Craigie, R. (1992) *J. Virol. 66*, 6361−6369.
8. Kulkosky, J., Jones, K. S., Katz, R. A., Mack, J. P. G., and Skalka, A. M. (1992) *Mol. Cell. Biol. 12*, 2331−2338.
9. Leavitt, A. D., Shiue, L., and Varmus, H. E. (1993) *J. Biol. Chem. 268*, 2113−2119.
10. Esposito, D., and Craigie, R. (1998) *EMBO J. 17*, 5832−5843.
11. Gerton, J. L., Ohgi, S., Olsen, M., Derisi, J., and Brown, P. O. (1998) *J. Virol. 72*, 5046−5055.
12. Heuer, T. S., and Brown, P. O. (1997) *Biochemistry 36*, 10655−10665.
13. Jenkins, T. M., Esposito, D., Engelman, A., and Craigie, R. (1997) *EMBO J. 16*, 6849−6859.
14. Engelman, A., Hickman, A. B., and Craigie, R. (1994) *J. Virol. 68*, 5911−5917.
15. Khan, E., Mack, J. P. G., Katz, R. A., Kulkosky, J., and Skalka, A. M. (1991) *Nucleic Acids Res. 19*, 851−860.
16. Puras Lutzke, R. A., Vink, C., and Plasterk, R. H. A. (1994) *Nucleic Acids Res. 22*, 4125−4131.
17. Vink, C., Oude Groemeger, A. M., and Plasterk, R. H. A. (1993) *Nucleic Acids Res. 21*, 1419−1425.
18. Vink, C., Puras Lutzke, R. A., and Plasterk, R. H. A. (1994) *Nucleic Acids Res. 22*, 4103−4110.
19. Woermer, A. M., and Marcus-Sekura, C. J. (1993) *Nucleic Acids Res. 21*, 3507−3511.
20. Cai, M., Zheng, R., Caffrey, M., Craigie, R., Clore, G. M., and Gronenborn, A. M. (1997) *Nat. Struct. Biol. 4*, 567−576.
21. Dyda, F., Hickman, A. B., Jenkins, T. M., Engelman, A., Craigie, R., and Davies, D. R. (1994) *Science 266*, 1981−1986.
22. Eijkelenboom, A. P., Sprangers, R., Hard, K., Puras Lutzke, R. A., Plasterk, R. H., Boelens, R., and Kaptein, R. (1999) *Proteins 36*, 556−564.

23. Goldgur, Y., Dyda, F., Hickman, A. B., Jenkins, T. M., Craigie, R., and Davies, D. R. (1998) *Proc. Natl. Acad. Sci. U.S.A. 95*, 9150−9154.
24. Greenwald, J., Le, V., Butler, S. L., Bushman, F. D., and Choe, S. (1999) *Biochemistry 38*, 8892−8898.
25. Lodi, P. J., Ernst, J. A., Kuszewski, J., Hickman, A. B., Engelman, A., Craigie, R., Clore, G. M., and Gronenborn, A. M. (1995) *Biochemistry 34*, 9826−9833.
26. Maignan, S., Guilloteau, J.-P., Zhou-Liu, Q., Clément-Mella, C., and Mikol, V. (1998) *J. Mol. Biol. 282*, 359−368.
27. Chow, S. A., Vincent, K. A., Ellison, V., and Brown, P. O. (1992) *Science 255*, 723−726.
28. Ellison, V., Gerton, J., Vincent, K. A., and Brown, P. O. (1995) *J. Biol. Chem. 270*, 3320−3326.
29. Engelman, A., Bushman, F. D., and Craigie, R. (1993) *EMBO J. 12*, 3269−3275.
30. van den Ent, F. M. I., Vos, A., and Plasterk, R. H. A. (1999) *J. Virol. 73*, 3176−3183.
31. van Gent, D. C., Vink, C., Oude Groeneger, A. A. M., and Plasterk, R. H. A. (1993) *EMBO J. 12*, 3261−3267.
32. Lee, S. P., and Han, M. K. (1996) *Biochemistry 35*, 3837−3844.
33. Lee, S. P., Xiao, J., Knutson, J. R., Lewis, M. S., and Han, M. K. (1997) *Biochemistry 36*, 173−180.
34. Wolfe, A. L., Felock, P. J., Hastings, J. C., Uncapher Blau, C., and Hazuda, D. J. (1996) *J. Virol. 70*, 1424−1432.
35. Jenkins, T. M., Engelman, A., Ghirlando, R., and Craigie, R. (1996) *J. Biol. Chem. 271*, 7712−7718.
36. Beechem, J. M. (1997) *Methods Enzymol. 278*, 24−49.
37. Lakowicz, J. R. (1999) *Principles of Fluorescence Spectroscopy*, 2nd ed., Plenum Press, New York.
38. Bilsel, O., Yang, L., Zitzewitz, J. A., Beechem, J. M., and Matthews, C. R. (1999) *Biochemistry 38*, 4177−4187.
39. Jones, B. E., Beechem, J. M., and Mathews, C. R. (1995) *Biochemistry 34*, 1867−1877.
40. Stockel, J., Doring, K., Malotka, J., Jahnig, F., and Dornmair, K. (1997) *Eur. J. Biochem. 248*, 684−691.
41. Dijkstra, D. S., Broos, J., Visser, A. J., van Hoek, A., and Robillard, G. T. (1997) *Biochemistry 36*, 4860−4866.
42. Liu, W., Chen, Y., Watrob, H., Barlett, S. G., Jen-Jacobson, L., and Barkley, M. D. (1998) *Biochemistry 37*, 15457−15465.
43. Moncrieffe, M. C., Eaton, S., Bajzer, Z., Haydock, C., Potter, J. D., Laue, T. M., and Prendergast, F. G. (1999) *J. Biol. Chem. 274*, 17464−17470.
44. Shen, F., Triezenberg, S. J., Hensley, P., Porter, D., and Knutson, J. R. (1996) *J. Biol. Chem. 271*, 4819−4826.
45. Bradrick, T. D., Beechem, J. M., and Howell, E. E. (1996) *Biochemistry 35*, 11414−11424.
46. Digris, A. V., Skakoun, V. V., Novikov, E. G., van Hoek, A., Claiborne, A., and Visser, A. J. (1999) *Eur. Biophys. J. 28*, 526−531.
47. Hauer, J. A., Taylor, S. S., and Johnson, D. A. (1999) *Biochemistry 38*, 6774−6780.
48. Kungl, A. J., Visser, N. V., van Hoek, A., Visser, A. J., Billich, A., Schilk, A., Gstach, H., and Auer, M. (1998) *Biochemistry 37*, 2778−2786.
49. Carver, T. E., Jr., and Millar, D. P. (1998) *Biochemistry 37*, 1898−1904.
50. Fernando, T., and Royer, C. (1992) *Biochemistry 31*, 3429−3441.
51. Lam, W. C., van der Schans, E. J., Joyce, C. M., and Millar, D. P. (1998) *Biochemistry 37*, 1513−1522.
52. Lam, W. C., Seifert, J. M., Amberger, F., Graf, C., Auer, M., and Millar, D. P. (1998) *Biochemistry 37*, 1800−1809.
53. Perez-Howard, G. N., Weil, P. A., and Beechem, J. M. (1995) *Biochemistry 34*, 8005−8017.
54. Brochon, J.-C., Tauc, P., Merola, F., and Schoot, B. M. (1993) *Anal. Chem. 65*, 1028−1034.
55. Graupner, M., Haalck, L., Spener, F., Lindner, H., Glatter, O., Paltauf, F., and Hermetter, A. (1999) *Biophys. J. 77*, 493−504.
56. Neyroz, P., Menna, C., Polverini, E., and Masotti, L. (1996) *J. Biol. Chem. 271*, 27249−27258.
57. Sopkova, J., Vincent, M., Takahashi, M., Lewit-Bentley, A., and Gallay, J. (1998) *Biochemistry 37*, 11962−11970.
58. Carteau, S., Mouscadet, J.-F., Goulaouic, H., Subra, F., and Auclair, C. (1993) *Arch. Biochem. Biophys. 300*, 756−760.
59. Sherman, P. A., and Fyfe, J. A. (1990) *Proc. Natl. Acad. Sci. U.S.A. 87*, 5119−5123.
60. Brochon, J.-C. (1994) *Methods Enzymol. 240*, 262−311.
61. Liversey, A. K., and Brochon, J.-C. (1987) *Biophys. J. 52*, 693−706.
62. Siemiarczuk, A., and Ware, W. R. (1989) *J. Phys. Chem. 93*, 7609−7618.
63. Valeur, B., and Weber, G. (1977) *Photochem. Photobiol. 25*, 441−444.
64. Hickman, A. B., Palmer, I., Engelman, A., Craigie, R., and Wingfield, P. (1994) *J. Biol. Chem. 269*, 29279−29287.
65. Yguerabide, J., Epstein, H. F., and Stryer, L. (1970) *J. Mol. Biol. 51*, 573−590.
66. Heuer, T. S., and Brown, P. O. (1998) *Biochemistry 37*, 6667−6678.
67. Pemberton, I. K., Buckle, M., and Buc, H. (1996) *J. Biol. Chem. 271*, 1498−1506.
68. Engelman, A., and Craigie, R. (1995) *J. Virol. 69*, 5908−5911.
69. Lee, S. P., Kim, H. G., Censullo, M. L., and Han, M. K. (1995) *Biochemistry 34*, 10205−10214.
70. Asante-Appiah, E., Seeholzer, S. H., and Skalka, A. M. (1998) *J. Biol. Chem. 273*, 35078−35087.
71. Asante-Appiah, E., and Skalka, A. M. (1997) *J. Biol. Chem. 272*, 16196−16205.
72. Coleman, J., Eaton, S., Merkel, G., Skalka, A. M., and Laue, T. (1999) *J. Biol. Chem. 274*, 32842−32846.
73. Leh, H., Brodin, P., Bischerour, J., Deprez, E., Tauc, P., Brochon, J.-C., LeCam, E., Couland, D., Auclair, C., and Mouscadet, J.-F. (2000) *Biochemistry 39*, 9285−9294.

BI000397J